ELSEVIER

Nuclear Instruments and Methods in Physics Research B 152 (1999) 1–11

NIM B
Beam Interactions with Materials & Atoms

Thick target neutron yields for the $^{7}Li(p,n)^{7}Be$ reaction near threshold

C.L. Lee *, X.-L. Zhou

Department of Nuclear Engineering, Massachusetts Institute of Technology, Cambridge, MA, USA

Received 25 June 1998; received in revised form 15 December 1998

Abstract

Transportable accelerator sources of epithermal neutrons are crucial for the development of hospital-based boron neutron capture therapy (BNCT) as a treatment modality for brain cancers. One method for producing such epithermal neutrons is near-threshold (p,n) reactions as studied by our group, as well as several other investigators. As part of this effort, we have developed accurate methods for computing the angular distributions and energy spectra of neutrons from thick targets using the $^{7}Li(p,n)^{7}Be$ reaction near threshold. Neutron yields are calculated for lithium metal as well as several lithium compounds of low molecular weight. The calculational method is discussed, with emphasis on the improvements over previously published methods. Neutron energy spectra, angular distributions, and total yields for proton beam energies up to 120 keV above threshold are presented. A method is also demonstrated for calculating neutron yields for targets that are not sufficiently thick to slow protons past the reaction threshold.

PACS: 29.25.Dz; 25.40.Qa; 27.20.+n
Keywords: Boron neutron capture therapy; Near-threshold BNCT; Thick target neutron production; $^{7}Li(p,n)^{7}Be$ reaction

1. Introduction

Boron neutron capture therapy (BNCT) is a binary cancer treatment modality. The treatment consists of two parts: (i) injection of a boronated compound, which preferentially concentrates in cancerous cells, into the patient, followed by (ii) irradiation of the tumor by thermal neutrons. The $^{10}B(n,\alpha)^{7}Li$ reaction, with its very large thermal neutron cross section, produces energetic heavy charged particles that provide highly localized dose deposition in the tumor, while the lower boron accumulation in surrounding healthy tissue results in relative sparing of these tissues [1].

For deep-seated tumors, thermal neutrons will not sufficiently penetrate the skull cap, depositing

* Corresponding author. Present address: X-CI, MS F663, Los Alamos National Laboratory, Los Alamos, NM 87545, USA. Tel.: +1 505 665 2849; fax: +1 505 665 8329; e-mail: chadlee@lanl.gov

0168-583X/99/$ – see front matter
PII: S0168-583X(99)00026-9

the bulk of their energy near the skin surface. For this reason, one of two approaches to BNCT is required: surgical resection of the skull cap so that the tumor site is exposed to a thermal neutron beam, or the use of a higher energy neutron beam [2]. Fast neutrons (greater than ~10 keV) are unacceptable for the second option because the neutron dose to the skin surface is unacceptably high and effectively limits the potential deliverable dose to the tumor. An epithermal beam, however, will penetrate the skull, moderating in the brain tissue and thermalizing near the tumor site without restrictively high skin doses. Epithermal beams thus allow patient treatment without surgical resection, though surgical debulking of the tumor usually takes place prior to treatment with BNCT. Previous work has established that the range of epithermal neutron energies ideal for BNCT is from ~1 eV to ~10 keV [3].

Because the energies of neutrons needed for BNCT are relatively low, moderation of the neutron source is required before delivery to the patient. Accelerator neutron sources, considered necessary for the successful implementation of BNCT in hospital settings, must be intense (to permit reasonable treatment times) and still provide an epithermal beam with small fast neutron, thermal neutron, and γ-ray contamination. A popular reaction considered for accelerator BNCT neutron sources is $^{7}Li(p,n)^{7}Be$ because the rapid rise of the cross section near threshold provides large quantities of relatively low energy neutrons. The cross section reaches 270 mb within 50 keV of the reaction threshold energy of 1.88 MeV, and a broad resonance centered at 2.25 MeV takes the cross section up to 580 mb [4]. Most past work by other researchers has concentrated on a proton bombarding energy of 2.50 MeV in order to take advantage of the resonance at 2.25 MeV [3]. This proton bombarding energy produces large neutron yields as the beam slows down in the lithium target, but the maximum and mean neutron energies are 787 and 326 keV, respectively. These beams require extensive moderation to reduce neutron energies to the epithermal region. These considerations have led our group to consider near-threshold BNCT as a viable alternative to conventional BNCT [5–7]. The proton bombarding energy is only several tens of keV above the reaction threshold, producing lower neutron yields but also beams with much lower mean energies, requiring much less moderation.

In the investigation of near-threshold BNCT, it is necessary to have an accurate method for computing thick target neutron yields. Specifically, both the energy spectrum and angular distribution of the neutrons produced by protons of a certain bombarding energy are required. It has been determined that the existing methods for computing thick target neutron yields are insufficient for accurate calculations over the range of incident proton energies of interest in this research. In particular, tabulated cross sections provide excellent data for energies above about 1.95 MeV, but the Jacobians used to calculate thick target neutron yields produce infinities close to the reaction threshold. Analytical forms of the differential cross section alleviate this problem close to threshold, but are incorrect for higher energies. A self-consistent method for producing differential thick target neutron yields for all proton energies below 2.50 MeV has been developed. This method has also been modified to determine neutron yields from compounds that contain lithium, as well as extending our method to partially thick targets. Partially thick targets are of sufficient thickness to result in significant proton energy loss, but are not sufficiently thick to slow the proton beam below the reaction threshold.

This article describes the method developed to generate the thick target differential neutron yields from near-threshold proton beams, focusing on the mathematical difficulties that arise for calculations within several keV of the reaction threshold and the techniques for overcoming these complexities. The results of calculations using this method are presented, including differential and total yields for thick and partially thick targets.

2. Theory

2.1. Near-threshold kinematics

As an illustration of the principles used in these calculations, consider a monoenergetic incident

proton beam with energy, E_{p_0}, of 1.95 MeV striking a thick lithium target. A thick target is defined to be sufficiently thick to slow protons past the reaction threshold. Fig. 1 provides kinematic relations between θ, the polar angle of emission of the neutron in the lab system; E_n, the lab neutron energy; and E_p, the lab proton energy that produced the neutron, for the ^{7}Li(p,n)^{7}Be reaction. This figure was produced with standard, non-relativistic kinematic equations involving the variables described above. Lines of constant E_p are plotted from E_{p_0} to $E_p = E_{th}$, the threshold energy of 1.88 MeV. When the proton beam impinges on a thick lithium target, the initial neutron yield will follow the energy and angle behavior shown on the uppermost contour. As the protons lose energy in the target, the energy and angular dependence of the neutron yield will be determined from contours of continuously decreasing proton energy, until neutrons are only produced in the forward direction at an energy of 29.7 keV at E_{th}. The neutron energy at threshold is determined from $E_n(E_{th}) = m_p m_n E_{th}/(m_{Be} + m_n)^2$, where m_p, m_n, and m_{Be} are the proton, neutron, and ^{7}Be nuclear masses. A thick lithium target will only produce neutrons with energies and angles corresponding to proton energies below E_{p_0}, i.e., neutrons will not be produced with energies and angles above the uppermost contour of Fig. 1. Note that for proton energies below

$$E_p^* = \frac{m_{Be}(m_{Be} + m_n - m_p)}{m_{Be}(m_{Be} + m_n - m_p) - m_p m_n} E_{th} = 1.92 \text{ MeV}, \quad (1)$$

neutron production is double-valued, giving two neutron energies for each angle of emission. In addition, neutrons are only produced in the forward direction ($\theta < 90°$).

It is clear from Fig. 1 that any combination of θ and E_n uniquely specifies E_p, and the differential neutron yield is therefore a pointwise function of these variables. This observation implies that it is not necessary to discretize the proton energy as the beam slows down in the target. The differential neutron yield at each proton energy is given by

$$\frac{d^2Y}{d\Omega\, dE_n}(\theta, E_n) = N_{^7\text{Li}} \frac{(d\sigma_{pn}/d\Omega')\,(d\Omega'/d\Omega)\,(dE_p/dE_n)}{(-dE_p/dx)}, \quad (2)$$

where $d^2Y/d\Omega\, dE_n$ is the differential neutron yield in units of neutrons per keV per steradian per millicoulomb, $N_{^7\text{Li}}$ is the ^{7}Li (target) atomic density, $d\sigma_{pn}/d\Omega'$ is the center-of-mass system (CM) differential (p,n) cross section, $d\Omega$ and $d\Omega'$ are differential solid angles in the lab and CM, respectively, and $-dE_p/dx$ is the proton stopping power in the target.

In order to have more compact notation in the following equations, it is useful to introduce two kinematic parameters, γ and ξ [8]. γ is defined as the ratio of the final CM speed to the CM speed of the neutron. The following expression for γ can be obtained from the nonrelativistic linear momentum and energy equations.

$$\gamma = \sqrt{\frac{m_p m_n}{m_{Be}(m_{Be} + m_n - m_p)} \left(\frac{E_p}{E_p - E_{th}}\right)}. \quad (3)$$

Note that as E_p approaches threshold, $\gamma \to \infty$, and for $E_p < E_p^*$, $\gamma > 1$. In addition, the parameter ξ is defined by

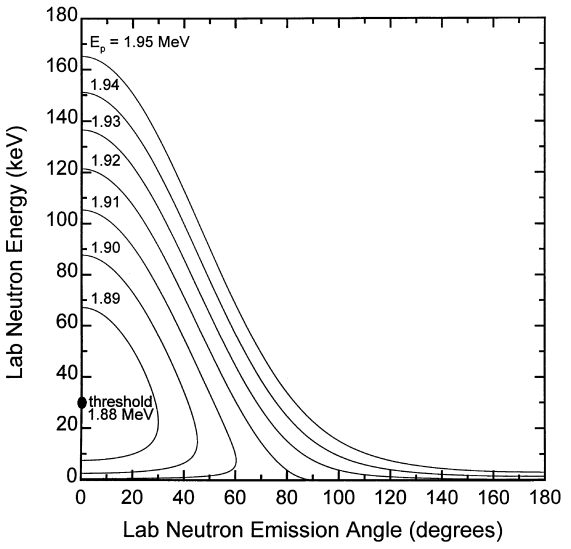

Fig. 1. Proton energy contours for a thick lithium target.

$$\xi^2 = 1/\gamma^2 - \sin^2\theta. \tag{4}$$

The first step in our determination of the thick target differential neutron yield is choosing a set of (θ, E_n) grid points at which $d^2Y/d\Omega\, dE_n$ is calculated. We generally use 1°, 1-keV intervals ranging from 0 to 180° and 0 to 250 keV. For each grid point, the proton energy E_p is calculated in a manner similar to that used to produce the contours of Fig. 1. Once E_p has been determined, γ, ξ, and the mass stopping power are determined, since these quantities are functions of E_p alone. The mass stopping power is determined from analytic formulas fit to experimental data [9].

Since the differential cross section $d\sigma_{pn}/d\Omega'$ is a function of the CM angle of emission, θ', the next step in the calculation is to determine the correct value of θ' corresponding to (θ, E_n). For $E_p > E_p^*$, neutron production is single-valued and

$$\theta' = \theta + \sin^{-1}(\gamma\ \sin\theta), \tag{5}$$

while for $E_p < E_p^*$, neutron production is double-valued and there are two possibilities for θ'. These CM angles, θ_1' and θ_2', are related to θ by

$$\theta_1' = \theta + \sin^{-1}(\gamma\ \sin\theta), \tag{6}$$

$$\theta_2' = \pi + \theta - \sin^{-1}(\gamma\ \sin\theta). \tag{7}$$

Note that θ_1' is the more forward-directed of these two angles and corresponds to higher neutron energies, while θ_2' is directed in the backward direction and corresponds to lower neutron energies. Now defining a neutron energy E_{equal}:

$$E_{equal} = (1+\gamma^2)E_n', \tag{8}$$

where E_n' is the CM neutron energy, given by

$$E_n' = \frac{m_{Be}(m_{Be} + m_n - m_p)}{(m_{Be}+m_n)^2}(E_p - E_{th}), \tag{9}$$

it is straightforward to demonstrate that for a given proton energy E_p, E_{equal} corresponds to the point where $\theta_1' = \theta_2' = \theta + 90°$. From the above statements, if $E_n \geqslant E_{equal}$ for the grid point in question, we must have θ_1' and Eq. (6) is calculated; if $E_n < E_{equal}$, θ_2' is the correct CM angle and Eq. (7) is used. Note from Eq. (6) that the maximum angle of emission for proton energies below E_p^* is given by $\theta_{max} = \sin^{-1}(1/\gamma)$.

It now remains to determine the CM differential cross section and the Jacobian transformations given in Eq. (2). These transformations are given by

$$\frac{d\Omega'}{d\Omega} = \pm\frac{\gamma}{\xi}(\cos\theta \pm \xi)^2, \tag{10}$$

$$\frac{dE_p}{dE_n} = \frac{1}{\cos\theta \pm \xi}\left[\frac{(m_{Be}+m_n)^2 E_p \xi}{m_p m_n E_p \xi(\cos\theta \pm \xi) \pm m_{Be}(m_{Be}+m_n-m_p)E_{th}}\right]. \tag{11}$$

In Eqs. (10) and (11), the + sign is used when $\theta' = \theta_1'$ and the − sign is used when $\theta' = \theta_2'$. Care must be taken in employing these expressions in various regions of (θ, E_n) space. For example, in the vicinity of θ_{max}, $d\Omega'/d\Omega \to \infty$ and $dE_p/dE_n \to 0$. This means that Eq. (2) is indeterminate at points where $\theta = \theta_{max}$, and this will create a computational problem for (θ, E_n) values at or close to these points. However, this problem can be easily remedied by considering the product of $d\Omega'/d\Omega$ and dE_p/dE_n, given by

$$\frac{d\Omega'}{d\Omega}\frac{dE_p}{dE_n} = \frac{\pm(m_{Be}+m_n)^2(\cos\theta \pm \xi)\gamma E_p}{m_p m_n E_p \xi(\cos\theta \pm \xi) \pm m_{Be}(m_{Be}+m_n-m_p)E_{th}}. \tag{12}$$

Now the limit for this product of Jacobians is given by

$$\lim_{\theta\to\theta_{max}} \frac{d\Omega'}{d\Omega}\frac{dE_p}{dE_n} = \frac{(m_{Be}+m_n)^2 E_p}{m_{Be}(m_{Be}+m_n-m_p)E_{th}}\sqrt{\gamma^2-1}. \tag{13}$$

Using the product of the Jacobian transformations therefore circumvents the computational problems that arise when calculating each transformation separately. For this reason, and since the expression for the Jacobian product has the simple closed form given in Eq. (12), this expres-

sion is used in all differential yield calculations. All calculational difficulties are not removed by the substitution given in Eq. (12). The greatest difficulty in near-threshold neutron yield calculations comes from the behavior of γ as $E_p \to E_{th}$: as pointed out earlier, γ becomes unbounded, and $d\Omega'/d\Omega\, dE_p/dE_n \to \infty$. We know that the CM differential cross section must go to zero at the reaction threshold, so Eq. (2) is still indeterminate $(0 \cdot \infty)$ at $E_p = E_{th}$. To understand how this problem is overcome, the particular aspects of the ^{7}Li(p,n)^{7}Be cross section near threshold must be considered.

In 1975, Liskien and Paulsen compiled extensive experimental cross section measurements from the existing literature and generated best fits to the data over the proton energy range from 1.95 to 7.0 MeV for both the reaction leading to the ground state of ^{7}Be and the first excited state, which has a threshold at 2.37 MeV [10]. These CM cross sections are given as Legendre polynomial expansions:

$$\frac{d\sigma_{pn}}{d\Omega'}(\theta') = \frac{d\sigma_{pn}}{d\Omega'}(0^\circ)\sum_{i=0}^{3} A_i(E_p)P_i(\cos\theta'). \tag{14}$$

The proton energy-dependent parameters A_0, A_1, A_2, A_3, and $d\sigma_{pn}/d\Omega'(0^\circ)$ are tabulated, making it extremely simple to use their fits for calculating reaction cross sections. In order to replicate the smooth variation of the cross section parameters with proton energy, cubic splines were fit through the data points given in Liskien and Paulsen's paper.

The tabulated cross section data from Liskien and Paulsen's paper are good for energies above 1.95 MeV, but they do not help us resolve the problem of indeterminacy near the reaction threshold. It is necessary to use an analytical form for the CM differential cross section to determine the actual near-threshold limits of the terms in Eq. (2). It has been pointed out by Gibbons and Macklin, as well as other sources [4,8,11–13], that the reaction cross section has the form expected from a broad s-wave resonance centered at about 1.93 MeV. The resulting form of the theoretical cross section is

$$\frac{d\sigma_{pn}}{d\Omega'} = A\frac{x}{E_p(1+x)^2}, \tag{15}$$

where $x = \Gamma_n/\Gamma_p$, the ratio of the neutron to proton channel widths, which has a functional form on the narrow energy range near threshold of $x = C_0\sqrt{1 - E_{th}/E_p}$, and C_0 and A are constants to be determined. We use $C_0 = 6$ to be consistent with the cross section data of Gibbons and Macklin. We have chosen a proton energy of 1.925 MeV as the boundary between tabulated and theoretical cross section values. This energy is roughly the upper limit of applicability of Eq. (15) (~50 keV above threshold), and the theoretical expression for $d\sigma_{pn}/d\Omega'$ has zero slope at this energy, making a smooth transition to the interpolated values a simple matter. Theoretical and interpolated cross section values agree at this energy if we set $A = 164.913$ mb MeV/sr.

Now using the definition of γ in Eq. (3), we may combine Eqs. (12) and (15) to give the cumbersome but useful formula

$$\frac{d\sigma_{pn}}{d\Omega'}\frac{d\Omega'}{d\Omega}\frac{dE_p}{dE_n} = \frac{\pm AC_0(m_{Be}+m_n)^2(\cos\theta \pm \xi)\sqrt{m_p m_n/m_{Be}(m_{Be}+m_n-m_p)}}{(1+x)^2[m_p m_n E_p \xi(\cos\theta \pm \xi) \pm m_{Be}(m_{Be}+m_n-m_p)E_{th}]} \tag{16}$$

for proton energies near threshold. Note that the threshold limit of Eq. (16) is a finite, non-zero value:

$$\lim_{E_p \to E_{th}} \frac{d\sigma_{pn}}{d\Omega'}\frac{d\Omega'}{d\Omega}\frac{dE_p}{dE_n} = \frac{AC_0(m_{Be}+m_n)^2\sqrt{m_p m_n/m_{Be}(m_{Be}+m_n-m_p)}}{m_{Be}(m_{Be}+m_n-m_p)E_{th}}. \tag{17}$$

For proton energies above the 1.925 MeV cutoff, the CM differential cross section is determined by interpolating the cross section parameters between their tabulated values using the cubic spline fits, and this is multiplied by the product of Jacobians given in Eq. (12). For proton energies below this cutoff, the expression given in Eq. (16) is used to determine the differential neutron yields. Finally,

using expressions for the ^{7}Li density in natural lithium metal, the thick target differential neutron yield is given by

$$\frac{\mathrm{d}^2 Y}{\mathrm{d}\Omega\,\mathrm{d}E_\mathrm{n}}(\theta, E_\mathrm{n}) = \frac{f_{^7\mathrm{Li}} N_0}{eA_\mathrm{eff}} \frac{\frac{\mathrm{d}\sigma_\mathrm{pn}}{\mathrm{d}\Omega'}\frac{\mathrm{d}\Omega'}{\mathrm{d}\Omega}\frac{\mathrm{d}E_\mathrm{p}}{\mathrm{d}E_\mathrm{n}}}{-\frac{1}{\rho}\frac{\mathrm{d}E_\mathrm{p}}{\mathrm{d}x}}, \tag{18}$$

where $f_{^7\mathrm{Li}}$ is the ^{7}Li atomic fraction in natural lithium metal (92.5%), N_0 is Avogadro's number, e is the electronic charge, and A_eff is the atomic weight of natural lithium metal.

2.2. Thick target neutron yield surface

Fig. 2 shows an example of a thick target differential neutron yield for 1.95 MeV incident proton energy. Note the smooth behavior of the yield surface in all regions of the calculation, due to the techniques described in the previous section. An irregular, jagged boundary edge between zero and non-zero yields is apparent in Fig. 2, which occurs because the yields are evaluated on a square array of grid points. There is actually a smooth line between the zero and non-zero values at the edge of the yield surface, which is the yield due to protons with an energy of precisely E_{p_0}, but because this line does not intersect the grid points where computed yield values are displayed, it is not visible as a smooth edge. The computer program that was written to implement this calculational technique is designed to calculate the location of this edge and the corresponding differential neutron yields, so that energy spectra and angular distributions are integrated smoothly.

Fig. 3 is a plot of the 0° thick target differential neutron yield for neutron energies between 0 and 150 keV. The calculations described previously have been modified in this plot to predict neutron yields for ^{7}Li metal, rather than natural lithium. The 0° differential yield shows good agreement with experimental data given by Kononov in his paper [14]. Error bars for these data were not given in the original reference. The rounding of the yield curve at threshold can be explained by the proton beam energy spread. For comparison, the same quantity is plotted using the tabulated data of Liskien and Paulsen for energies below 1.95 MeV. The incorrect values very close to the reaction threshold are not due to incorrect cross section values given in Liskien and Paulsen's paper; rather, they are due to the inability of any tabulated cross section data to work near threshold because of the mathematical problems that occur in this region.

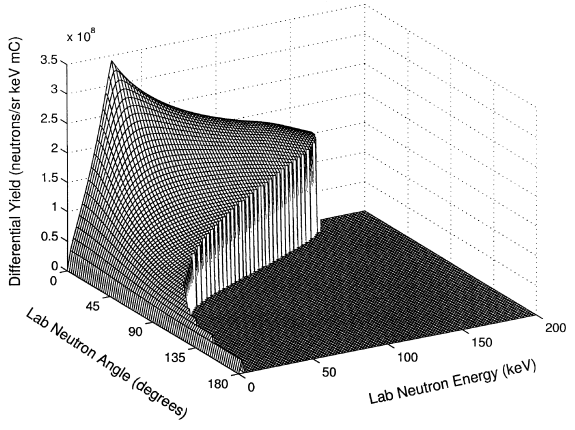

Fig. 2. Differential neutron yield for 1.95 MeV protons incident on natural lithium metal.

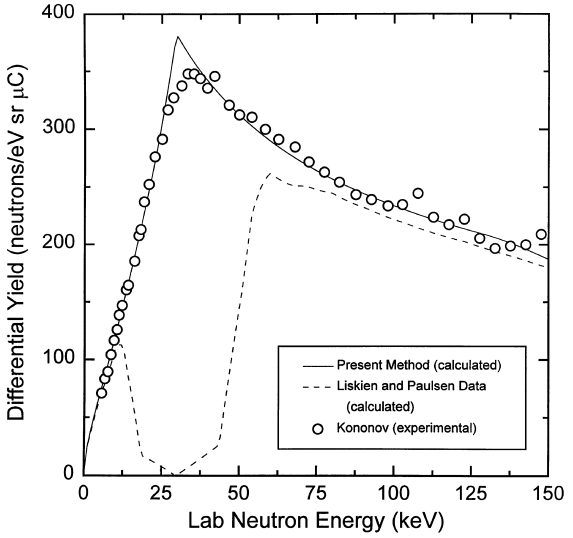

Fig. 3. A comparison of 0° thick target neutron yields.

2.3. Thick target neutron energy spectra and angular distributions

It is straightforward to calculate thick target neutron energy spectra and angular distributions by integrating Eq. (2) over solid angle and energy, respectively:

$$\frac{\mathrm{d}Y}{\mathrm{d}E_\mathrm{n}}(E_\mathrm{n}) = 2\pi \int_0^{\theta_{\max}(E_{\mathrm{p}_0})} \frac{\mathrm{d}^2Y}{\mathrm{d}\Omega\,\mathrm{d}E_\mathrm{n}}(\theta, E_\mathrm{n})\ \sin\theta\,\mathrm{d}\theta, \tag{19}$$

$$\frac{\mathrm{d}Y}{\mathrm{d}\Omega}(\theta) = \int_{E_{\mathrm{n,min}}}^{E_{\mathrm{n,max}}(E_{\mathrm{p}_0})} \frac{\mathrm{d}^2Y}{\mathrm{d}\Omega\,\mathrm{d}E_\mathrm{n}}(\theta, E_\mathrm{n})\,\mathrm{d}E_\mathrm{n}. \tag{20}$$

Thick target neutron energy spectra produced for near-threshold energies using Eq. (19) are shown in Fig. 4, which gives the energy spectra for incident proton energies in steps of 10 keV between 1.89 and 2.00 MeV. Note that there is no unusual behavior around 30 keV (E_n at the reaction threshold), where other yield computation techniques can produce erroneous spikes due to the infinity in the Jacobian product. The accuracy of these energy spectra should only be limited by the accuracy of the experimental cross section data, the nuclear masses, the mass stopping power, numerical round-off error, and errors incurred by integrating using the trapezoidal method, all of which are expected to be small.

Fig. 5 gives the thick target neutron angular distributions for incident proton energies between 1.89 and 2.00 MeV. These distributions were determined as shown in Eq. (20). A logarithmic scale has been used for the angular distributions in order to show the extremely low yields in backward emission directions. For incident proton energies below E_p^*, no neutrons are produced for angles greater than $\theta_{\max}(E_{\mathrm{p}_0})$, as expected.

It is important to note that while the differential neutron angular yield, $\mathrm{d}Y/\mathrm{d}\Omega(\theta)$, with units of neutrons/sr mC, in Fig. 5 is peaked in the 0° direction, the peak in the actual neutron emission spectrum will not be in the forward direction. In fact, there will be no neutrons emitted in the 0° direction. This may be seen in Fig. 6, where the angular distributions of Fig. 5 are multiplied by the $2\pi\sin\theta$ term from the solid angle differential element. The differential neutron yield in Fig. 6 is therefore given in units of neutrons/degree mC, and the neutron yield between two angles θ_1 and θ_2 is simply given by the integral of this new yield

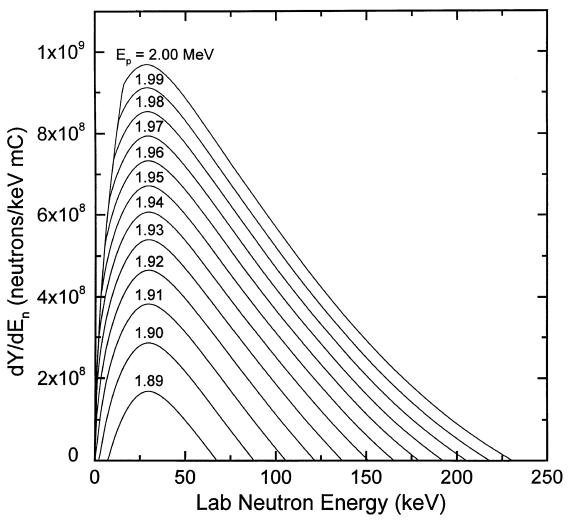

Fig. 4. Near-threshold thick target neutron energy spectra for natural lithium metal.

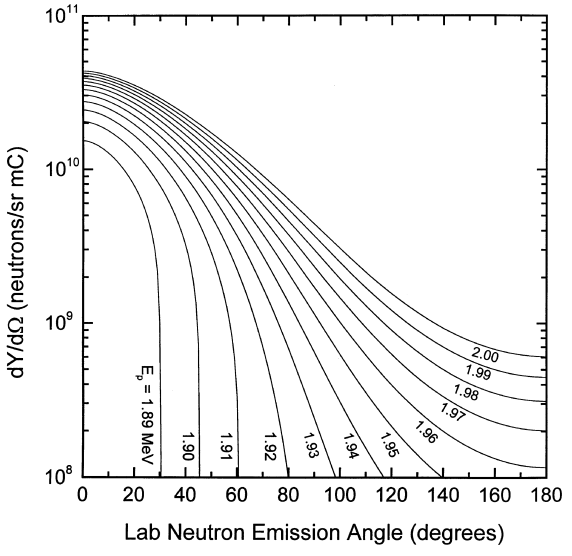

Fig. 5. Near-threshold thick target neutron angular distributions for natural lithium metal.

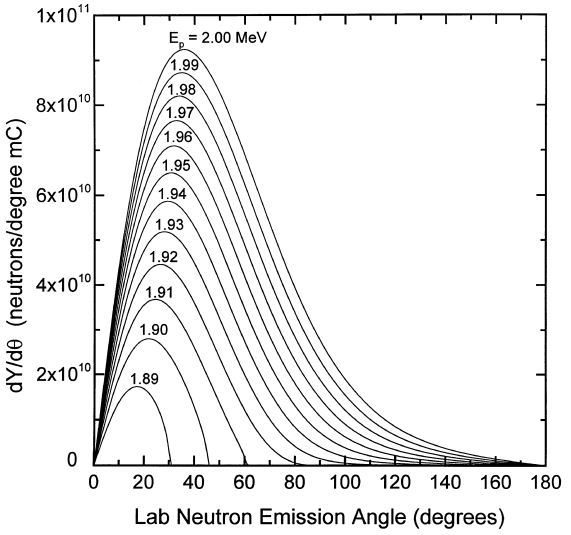

Fig. 6. Near-threshold thick target neutron angular yields for natural lithium metal. These yields, with units of neutrons/degree mC, are obtained by multiplication of the angular distributions of Fig. 5 by the solid angle differential element.

function over θ. The $\sin\theta$ term from the solid angle element forces the yield to go to zero in the forward direction, and the maximum yields in the near-threshold region are seen to be in the 20–40° range.

2.4. Thick target total neutron yields

Integrating the thick target differential neutron yields over both neutron energy and solid angle gives the total neutron yields for the various incident proton energies. Table 1 gives total thick target neutron yields, maximum and mean neutron energies over all angles, and maximum and mean emission angles over all energies.

2.5. Application to lithium compounds

It is a relatively simple matter to modify Eq. (18) to predict neutron yields in lithium compounds. The A_{eff} term must be changed to correspond to the molecular weight of the lithium compound, and in addition it is necessary to multiply by n, the number of lithium atoms per unit cell of the compound. For example, in the case of lithium oxide, Li_2O, there are two lithium atoms per molecular unit, so $n = 2$ and the molecular weight of Li_2O is used for A_{eff}. Unless the ^{7}Li enrichment is changed, $f_{^7\text{Li}}$ will not change. The only other change in calculating yields for lithium compounds is in the mass stopping power, which in the absence of experimental data must be

Table 1
Near-threshold thick target neutron yields for lithium metal

Incident proton energy (MeV)	Total neutron yield (n/mC)	Maximum neutron energy (keV)	Mean neutron energy (keV)	Maximum neutron angle (degrees)	Mean neutron angle (degrees)
1.89	6.34E9	67.1	34.0	30.0	16.5
1.90	1.49E10	87.6	38.3	45.2	23.0
1.91	2.41E10	105.3	42.4	60.3	27.8
1.92	3.35E10	121.4	46.5	180	31.9
1.93	4.30E10	136.6	50.6	180	35.3
1.94	5.25E10	151.1	54.4	180	38.3
1.95	6.21E10	165.1	58.1	180	41.0
1.96	7.16E10	178.8	61.6	180	43.5
1.97	8.12E10	192.1	65.0	180	45.6
1.98	9.08E10	205.1	68.4	180	47.6
1.99	1.00E11	218.0	71.7	180	49.4
2.00	1.10E11	230.6	75.1	180	51.1
2.10	2.13E11	350.4	108.4	180	63.0
2.20	3.62E11	463.4	158.9	180	68.7
2.30	5.78E11	573.1	233.1	180	66.3
2.40	7.48E11	680.6	286.5	180	63.8
2.50	8.83E11	786.7	326.4	180	62.9

estimated from the addivity rule for stopping powers. Our proton energy range of interest falls in the region of greatest applicability of the Bethe–Bloch formula [15], so that the Bragg–Kleeman rule is generally applicable [16–18]. Unlike lithium metal, lithium compound stopping powers are tabulated at particular proton energies, and linear interpolation is used to determine the stopping power at energies between these tabulated values. Tabulated elemental stopping powers used to construct compound stopping powers were taken from Janni [15].

Thick target yields have been calculated for Li_3N, Li_2O, LiF, LiOH, and LiH. These compounds were chosen to have high lithium atom densities and low molecular weights. Although the lithium atom density is higher for all compounds listed above except LiOH, the neutron yields are lower than for lithium metal targets. This is due to the larger stopping powers and masses that appear in the denominator of Eq. (18). The angular distributions and energy spectra of lithium compound neutrons are generally similar to those of lithium metal because the stopping powers of all elements have the same general energy variation on the proton energy range of interest, so the compound stopping powers also have the same energy variation. A comparison of thick target neutron yields for several compounds is given in Table 2.

Table 2
Near-threshold thick target neutron yields for lithium compounds (yields are in units of neutrons/mC)

Incident proton energy (MeV)	Li	LiF	Li_2O
1.89	6.34E9	1.92E9	3.11E9
1.90	1.49E10	4.52E9	7.33E9
1.91	2.41E10	7.29E9	1.18E10
1.92	3.35E10	1.01E10	1.64E10
1.93	4.30E10	1.30E10	2.11E10
1.94	5.25E10	1.57E10	2.57E10
1.95	6.21E10	1.88E10	3.04E10
1.96	7.16E10	2.17E10	3.51E10
1.97	8.12E10	2.45E10	3.98E10
1.98	9.08E10	2.75E10	4.45E10
1.99	1.00E11	3.04E10	4.93E10
2.00	1.10E11	3.33E10	5.40E10

2.6. Partially thick targets

This technique is well suited to the prediction of neutron yields from targets that are not sufficiently thick to slow the proton beam past the reaction threshold. Consider a proton beam passing through a partially thick target of thickness Δx. As the beam passes through the target, the mean beam energy decreases until it exits the lithium metal or compound with a mean beam energy of $E_{p,exit} > E_{th}$. Fig. 7 is similar in composition to Fig. 1, except that only contours for E_{p_0} and $E_{p,exit}$ are shown. Since the proton beam leaves the target before reaching energies below $E_{p,exit}$, the differential neutron yield for proton energies below this is zero. Neutrons will only be produced in the region bounded by these contours, but in all other ways, this calculation is identical to the one described before. It only remains to determine $E_{p,exit}$.

Consider a function $\mathscr{R}_i(E_p)$, defined as the range of protons of energy E_p in material i. After passing through a partially thick target, the range

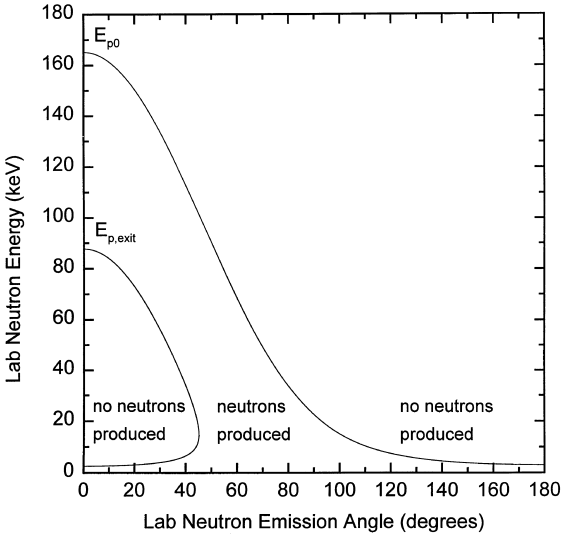

Fig. 7. Contours defining neutron production in a partially thick target. Neutrons are only produced with energy and angle combinations between the upper and lower contours.

is reduced and we may invert this function to determine the exit energy:

$$E_{\mathrm{p,exit}} = \mathscr{R}_i^{-1}[\mathscr{R}_i(E_{\mathrm{p}_0}) - \Delta x], \tag{21}$$

where $\mathscr{R}_i^{-1}(x)$ is the proton energy whose range in material i is x. This method is applicable for small target thicknesses such that range and path-length straggling are not appreciable. In this research, the range is well fit to a least squares quadratic, which is easily inverted by finding the roots of the quadratic.

Fig. 8 shows total neutron yields as a function of proton beam energy for several partially thick targets in LiF. Note that there is an abrupt bend in the yield at a proton energy that is characteristic of the target thickness. The total yield levels out, decreasing only slightly for higher proton energies. This may be understood by considering the expression for total neutron yield from a partially thick target, Y_{partial}:

$$Y_{\mathrm{partial}} = \frac{f_{7\mathrm{Li}} N_0}{eA_{\mathrm{eff}}} \int_{E_{\mathrm{p,exit}}}^{E_{\mathrm{p}_0}} \frac{\sigma_{\mathrm{pn}}(E_{\mathrm{p}})}{-\frac{1}{\rho}\frac{\mathrm{d}E_{\mathrm{p}}}{\mathrm{d}x}}\,\mathrm{d}E_{\mathrm{p}}. \tag{22}$$

Since neither the total (p,n) cross section nor the mass stopping power changes appreciably for proton energies between 1.93 and 2.00 MeV, the total yield is expected to remain constant over this range. It is important to note, however, that since the location of the contour for $E_{\mathrm{p,exit}}$ will change, for a given target thickness, as the incident proton energy changes, the energy spectrum and angular distribution of the neutron yield will also change (see Fig. 7).

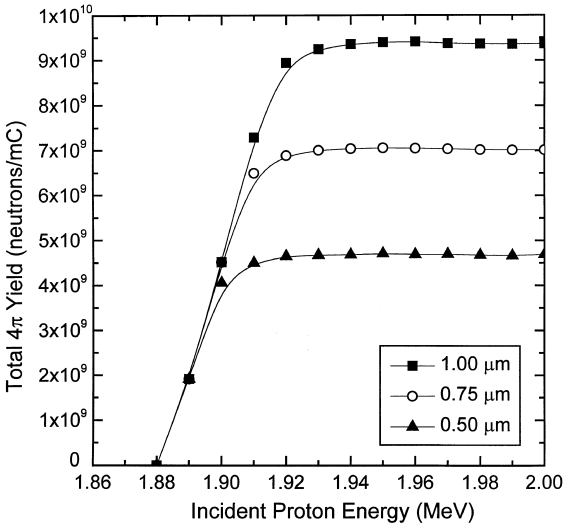

Fig. 8. Total neutron yields for partially thick LiF targets.

3. Summary

This report has given a detailed description of the method developed for determining thick target neutron yields from the ^{7}Li(p,n)^{7}Be reaction near the reaction threshold. This technique is particularly useful for the differential neutron yield in angle and energy, since the results do not depend on any discretization of the angle of emission, neutron energy, or proton beam energy in the target. In fact, Eq. (2) may be used to calculate the neutron yield at a particular value of θ and E_{n} without having to follow the entire slowing down history of the proton beam. The yields were developed using exact (non-relativistic) kinematic relations in such a way that the only error in the yields should be due to errors in the nuclear masses, stopping powers, cross section parameters, and trapezoidal integration in the case of energy spectra and angular distributions. Pathologies in the yield expression that arise in certain regions of the (θ, E_{n}) plane are removed using this technique, so numerical artifacts such as spikes in the differential yield are eliminated.

References

[1] G.L. Locher, Am. J. Roentgenol. 36 (1936) 1.
[2] R.F. Barth, A.H. Soloway, J. Neuro-Onco. 33 (1997) 3.
[3] J.C. Yanch et al., Med. Phys. 19 (1992) 709.
[4] J.H. Gibbons, R.L. Macklin, Phys. Rev. 114 (1959) 571.
[5] J.F. Harmon et. al., in: Proceedings of the 14th International Conference on the Application of Accelerators in Research and Industry, 1996.
[6] X.-L Zhou, C. Lee, Appl. Rad. Isot. 48 (1997) 1493.
[7] R.J. Kudchadker, Optimized accelerator based epithermal neutron beams for boron neutron capture therapy, Ph.D. Dissertation, University of Missouri–Columbia, 1996.
[8] A.I.M. Ritchie, J. Phys. D 9 (1976) 15.
[9] H.H. Andersen, J.F. Ziegler, Hydrogen: Stopping powers and ranges in all elements, Pergamon Press, New York, 1985.

[10] H. Liskien, A. Paulsen, At. Data Nucl. Data Tables 15 (1975) 57.
[11] H.H. Barschall et al., Neutron sources for basic physics and applications, Pergamon Press, New York, 1983.
[12] J.B. Marion, J.L. Fowler, Fast Neutron Physics, Interscience, New York, 1997.
[13] K.K. Sekharan et al., Nucl. Instr. Meth. 133 (1976) 253.
[14] V.N. Kononov et al., At. Energ. 43 (1977) 303.
[15] J.F. Janni, At. Data Nucl. Data Tables 27 (1982) 147.
[16] G.N. Potetyunko, At. Energ. 52 (1982) 129.
[17] D.I. Thwaites, Nucl. Instr. Meth. B 12 (1985) 84.
[18] J.F. Ziegler, J.M. Manoyan, Nucl. Instr. Meth. B 35 (1988) 215.